Autonomous Robotic System for Thermographic Detection of Defects in Upper Layers of Carbon Fiber Reinforced Polymers*

Morris Antonello, Stefano Ghidoni and Emanuele Menegatti

Abstract— **Carbon Fiber Reinforced Polymers (CFRPs) are composites whose interesting properties, like high strength-to-weight ratio and rigidity, are of interest in many industrial fields. Many defects affecting their production process are due to the wrong distribution of the thermosetting polymer in the upper layers. In this work, they are effectively and efficiently detected by automatically analyzing the thermographic images obtained by Pulsed Phase Thermography (PPT) and comparing them with a defect-free reference. The flash lamp and infrared camera needed by PPT are mounted on an industrial robot so that surfaces of CFRP automotive components, car side blades in our case, can be inspected in a series of static tests. The thermographic image analysis is based on local contrast adjustment via UnSharp Masking (USM) and takes also advantage of the high level of knowledge of the entire system provided by the calibration procedures. This system could replace manual inspection leading to a substantial increase in efficiency.**

Fig. 1. Complete experimental setup with robot, infrared camera, flash lamp and CFRP.

I. INTRODUCTION

Increasing use of Carbon Fiber Reinforced Polymers (CFRPs) is required whenever high strength-to-weight ratio and rigidity are necessary, as it happens in some application fields like automotive, aerospace and civil engineering, sports goods and military applications. Carbon fiber is made of long strings of carbon atoms that can be woven together to form sheets. Such sheets can be layered onto each other and joined together by means of a glue layer, to be placed between every couple of adjacent carbon sheets; the whole structure is then filled with polymer to create CFRPs. Carbon fiber is the reinforcement, which provides the strength, while the thermosetting polymer, e.g. epoxy resin, is the matrix, which binds the reinforcements together [11]. CFRPs can be manufactured using a number of techniques, all of which aim to combine the fiber and resin into a well-consolidated product. Several types of defects can affect the production process, including porosity, foreign bodies, incorrect fiber volume fraction due to excess or insufficient resin and bonding effects [16]. Defects can also occur in the placement of the glue between consecutive carbon fiber sheets.

Detecting defects in CFRPs is one of the goals of the European project Thermobot[1], which aims at replacing manual inspection in order to achieve better efficiency and performance in the production phase. The research leading to the results presented in this paper is part of this project, and

aims at inspecting the glue layer that bonds together carbon fiber sheets. Even though such layer is inside the part to be inspected, thermography, in particular the technique named Pulsed Phase Thermography (PPT) [12], [13] is capable of revealing the glue disposition, thus enabling the inspection.

Three modules have been developed for the whole project: thermographic inspection, robot path planning and thermal image analysis. PPT enables the nondestructive testing and evaluation (NDT&E) of CFRPs. The data acquisition setup consists of a flash lamp, the Hensel EH Pro 6000 with its power supply Tria 6000-S, and an infrared camera, the ImageIR 8300 by InfraTec GmbH. The flash lamp is an external source of energy which applies a short thermal pulse inducing a temperature difference between areas with different distribution of glue in the specimen under examination. The thermal changes on the surface are captured by the infrared camera. The flash, whose power can be set, overpowers the ambient light making the acquisition process controllable. The flash lamp and infrared camera are mounted on an industrial robot, the Stäubli TX90L with the CS8C controller, in order to inspect parts larger than the field of view of the camera. In particular, the surface of CFRP components are inspected in a series of static tests from a number of points of view such that the entire perimeter of the part can be covered. Indeed, the perimeter is more interesting than the rest of the part because the glue is distributed along the edge. The system is depicted in Fig. 1; the inspected component is a car side blade manufactured by one of the partners of the project, Benteler-SGL. Images are acquired for each point of view and then processed for obtaining the PPT phase images. Their analysis for revealing defective areas is the main focus of this paper. It is addressed by taking advantage of the high level of knowledge of the

entire system provided by the calibrations [6] and adapting an image sharpening technique well-known in photography, the UnSharp Masking (USM). Since the bonding cannot be simulated, defects are revealed by comparing each PPT phase image with the respective defect-free reference. The imaging process is as controllable as the acquisition given the repeatability of the workcell conditions. In summary, the main contributions of this paper are:

- an automatic robotic system for the detection of defects in the upper layers of CFRPs;
- a thermographic analysis of CFRPs based on PPT;
- the PPT phase image analysis exploiting USM and the high level of knowledge and control of the real workcell;
- the defect detection by comparison with a fault-free reference.

The detection of internal cracks cannot be performed since the required amount of heat generated by the flash lamp would be so high that it would damage the inspected object.

This paper is structured as follows. In Section II, the starting points for the analysis and comparison of PPT phase images are outlined by revising the state of the art. The core of the visual inspection system that enables the detection of defects is detailed in Section III. The results obtained during the experiments are described in Section IV. Finally, in Section V, the main conclusions are drawn and some final remarks reported.

II. STATE OF THE ART

Many works deal with the applicability of infrared thermography for NDT&E. Some of them compare multiple thermography techniques [9], while others focus on one of them, for example PPT [10]. In any case, these techniques have been applied to various case studies, including detection of defects in stainless steel and aluminium [1] or glue deficiency in laminated wood [3] and for superficial defects in multi-layered composites used in military applications [18]. Furthermore, infrared imaging in medicine has been around since the early 1970s and its application is being investigated for breast cancer [4], burn trauma, diabetes, vascular problems, and neurological problems [8]. In all quoted studies, apart [4], the focus in on the thermography technique itself: thermographic images are calculated and then inspected manually. Instead, the focus of this work is on the automatic defect detection, that is achieved by means of thermo-image analysis and comparison to the reference. To address these tasks, the OpenCV library [5], which includes comprehensive set of both classic and state-of-the-art computer vision and machine learning algorithms, is a good starting point. The first goal is the detection of a region of interest in each PPT phase image, knowing that only the comparison of the glued areas (which appear darker), is of concern. The second is the comparison between PPT phase image and reference, which is restricted to the Regions Of Interest (ROI) evaluated in the previous step. The methods to solve the former problem will be simpler than those addressing similar problems like background/foreground extraction [15], image matting or saliency detection [7] and will not need user
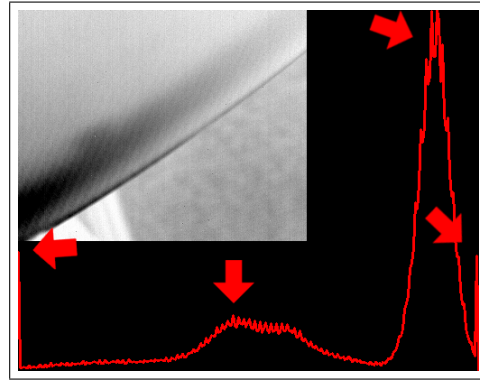

Fig. 2. A PPT phase image (top-left) and its brightness histogram. There are four main peaks denoting that Otsu's binarization cannot be applied because the image is not bimodal.

interaction. Indeed, the texture in the involved PPT phase images is also simpler than in the images usually employed for validating those techniques, for example outdoor pictures of people with hair blown by the wind. The same holds for the latter problem. Every PPT phase image will be compared with a defect-free reference previously taken from the same point of view, so that the comparison methods do not need to cover rotations, translations or scalings.

III. METHODS

This section focuses on the description of the comparison between two PPT phase images. They are gray-scale images, like the one in the top-left corner of Fig. 2, in which darker shades of gray denote the presence of glue. This process is characterized by three main steps displayed from left to right in Fig. 3:

1) foreground extraction from PPT phase images;
2) detection of adhesive bondings in CFRP;
3) pairwise comparison of adhesive bondings for difference detection.

The first two aim at restricting the comparison to a region of interest with glue in order to minimize false positives and false negatives. A simpler pixel-by-pixel comparison would be unreliable because of the differences in the carbon fiber texture.

A. Foreground Extraction from PPT Phase Images

Two complementary regions can be found in each image, one corresponding to the CFRP part in the foreground and the other to the background. As shown in the CFRP part in Fig. 2, both regions might have non-uniform brightness distribution because the glue might not be uniformly distributed on the surface and the distance of each point in the background from the infrared camera might vary. Of course, a way to binarize images and extract foreground is of concern. As a consequence of non-uniform brightness distribution in both regions, not only is simple thresholding not accurate, but also no threshold can be automatically calculated from image histograms, e.g. by means of the Otsu's binarization [14]. Indeed, images are not bimodal as
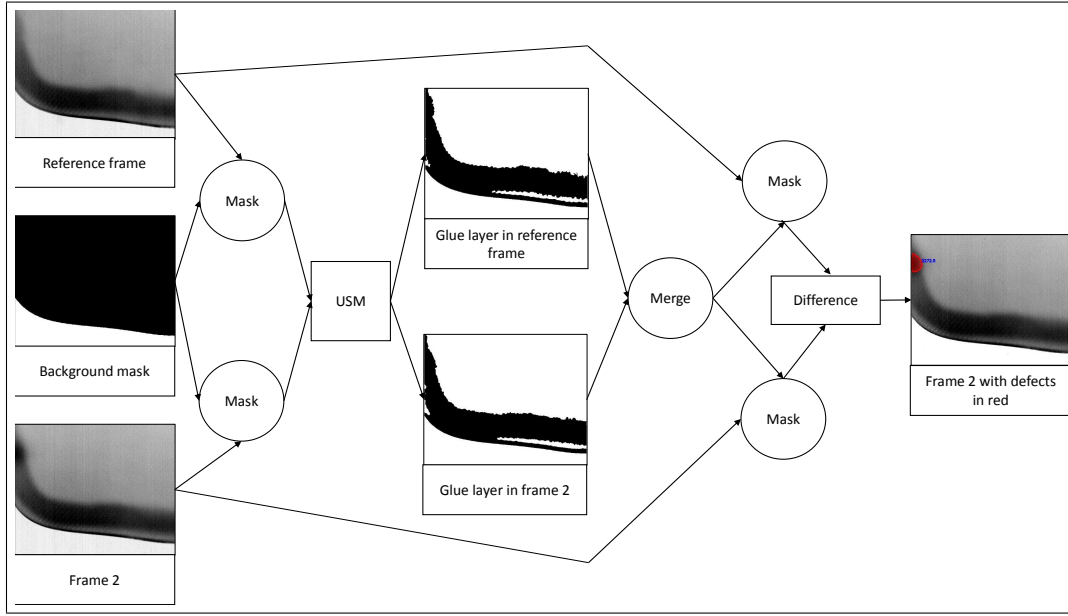
Fig. 3. Flowchart illustrating the comparison process of two PPT phase images. This process is characterized by three main steps displayed from left to right: foreground extraction from PPT phase images, detection of adhesive bondings in foregrounds and pairwise comparison of adhesive bondings for difference detection.

demonstrated by counting the number of main peaks in the brightness histogram shown in Fig. 2.

Viable alternatives are to be evaluated. One of them is the knowledge-based approach [6] by means of the high level of knowledge of the experimental setup and the backward projection [2] of each image point onto the 3D polygon mesh model of the CFRP part. The model, view and projection transformation matrices, whose composition is the mapping from the part space to the image space, are all well-known. These pieces of information come from three preliminary calibrations that respectively lead to the knowledge of the camera parameters, the position of the camera with respect to the robot, and the position of the robot with respect to the part. In this way, the foreground extraction is performed by evaluating for each image point the intersection between the 3D model of the part and the ray passing through that image point and the focal point. If the ray intersects the 3D model, the image point falls on the part and belongs to the foreground, otherwise it does not fall on the part and belongs to the background. The backward projections of every image point can be expensive, but masks are created only once and for all once for each of the fixed positions.

As another option, if these matrices are not available, the foreground can be extracted with minimal user interaction running the GrabCut algorithm [15] freely available in OpenCV. This algorithm starts with a user-specified bounding box around the foreground region and some hints on background and foreground pixels inside of it. Then it creates the background/foreground segmentation. The system combines hard segmentation by iterative graph-cut optimization with border matting to deal with blur and mixed pixels on object boundaries. Obviously, this latter approach, which requires interaction with the user, is more tedious.

B. Detection of Adhesive Bondings in CFRP

Dark shades of gray denote the layer of glue. Nevertheless, the definition of dark area is not straightforward and cannot rely on simple thresholding: first of all, the chosen value would not be the best for each image in the dataset, given the non-homogeneity of the glue layer in the CFRP part; second, illumination might not be uniform over the whole CFRP part. These remarks about brightness values hold mostly when comparing images taken from different points of view and secondarily when comparing different regions of an image. Hence, what is required for the detection of the glue layers is an approach that takes into account brightness gradients: this way, it is possible to detect dark regions compared to their surroundings. For this kind of analysis, an approach based on local contrast adjustment has been studied and developed. This approach is performed in four steps:

1) noise filtering;
2) unsharp masking;
3) thresholding;
4) artifact filtering.

The core of the algorithm is the unsharp masking, which is not applied standalone because it could enhance unwanted details due to ISO noise or film grain, as in the blue box in Fig. 4(a), and vertical banding noise, as in the red box in Fig. 4(a). In addition, also artifacts like the carbon fiber pattern itself, Fig. 4(b), could be strongly highlighted. This can be made up for by adding two steps, a pre-processing and a post-processing filtering.

The pre-processing is a soft median filter which proved to eliminate vertical noise more effectively than a Gaussian filter. An aperture size of 13 px is an appropriate trade-off between noise removal and level of detail. The starting frame is depicted in Fig. 5(a) and its blurred copy in Fig. 5(b).
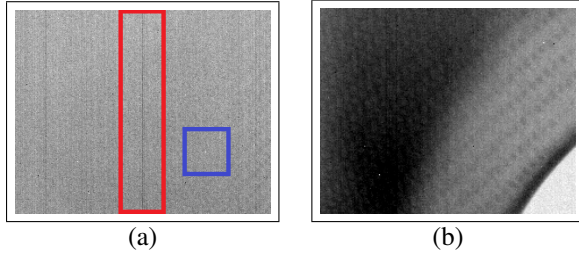
Fig. 4. Examples of noise: ISO noise or film grain in the blue box (a), vertical banding noise in the red box (a) and carbon fiber pattern (b).

UnSharp Masking (USM) is an image sharpening technique well-known in photography. Let O be the input image, in this case the softly blurred copy of the starting frame obtained after the pre-processing step, and B its blurred copy. The blur can be a 2D Gaussian blur with a certain aperture size, the radius r. The method consists in calculating an unsharp mask U, the difference between the original image O and its blurred copy B as shown in Eq. 1, and an high contrast version of the original image C, the sharpened difference between the original image O and its blurred copy B as shown in Eq. 2. The amount of overshoot, namely how much contrast is added, can be set via the parameter a.

$$U = |O - B| \tag{1}$$

$$C = a * O - a * B \tag{2}$$

In Fig. 5, the intermediate images are reported: O (b), B (c), U (d) and C (e). The unsharp mask U roughly points out the contours, which are sharpened in the high contrast image C. The sharpened image S is the sum of the original image O and the high contrast image C, optionally masked with the unsharp mask U by setting the threshold th, see Eq. 3. Given a 2D point P_U on the unsharp mask U, let I_{P_U} be its intensity of gray varying from 0 to 255:

$$S = \begin{cases} O & \text{if } I_{P_U} < th \\ O + C & \text{otherwise.} \end{cases} \tag{3}$$

The parameter th is the minimum difference in pixel values that indicates an edge to which some sharpen must be applied to protect areas of smooth tonal transition from sharpening. If it is set to 0, the unsharp mask U is not taken into account. The sharpened image S is depicted in Fig. 6(a). The choice of the three parameters, the radius r, the amount a and the threshold th, is important. This technique can increase either sharpness or local contrast. Indeed, they are both forms of differences, respectively small-scale (high-frequency) and large-scale (low-frequency), the latter of which are of concern. They can be increased using high radius and amount. Good values are 99 px for r and 25 for a. The third parameter, the threshold th, is not as crucial as the other two and can be set to 0.

Rather, the thresholding of S is of interest since only dark regions are to be kept, see Fig. 6(b). A good value is 180.
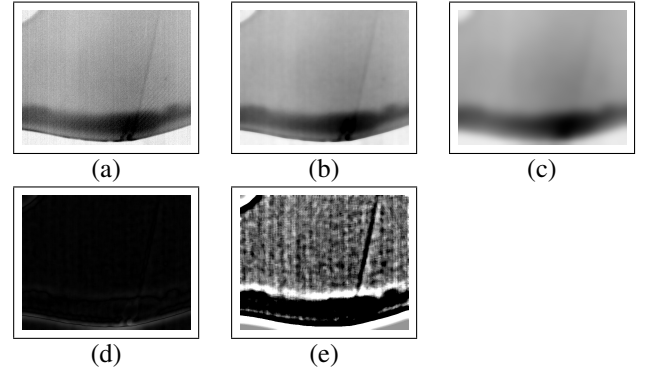

Fig. 5. Unsharp masking is based on the simple detection of contours performed by subtracting blurriness B from the initial frame O. From left to right: initial frame (a), initial frame after soft Gaussian blurring O (b), O after heavy Gaussian blurring B (c), unsharp mask U (d) and high contrast image C (e).
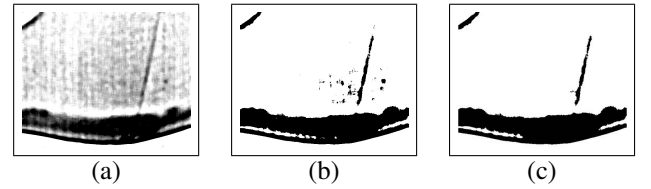

Fig. 6. Postprocessing after unsharp masking. From left to right: the sharpened frame S obtained by unsharp masking (a), after thresholding (b) and after the last post-processing step for removing artifacts characterized by small contours (c).

The post-processing is a final check useful for removing possible remaining artifacts characterized by small contours. The function retrieves contours using the algorithm described in [17], already implemented in OpenCV. The final result looks like Fig. 6(c) and provides the region of interest for the comparison in the next step.

C. Pairwise Comparison of Adhesive Bondings for Difference Detection

This step uses the masks built in the previous step in order to restrict the comparison to a region of interest with glue to minimize false positives and false negatives. Let A and B be the two images to be compared and M the union of the two masks obtained following the procedure explained in the previous step. First of all, a Gaussian or median filter is applied to obtain both C and D images. This blur should be soft (e.g. Gaussian with aperture size 29 px) otherwise differences in the shapes of the layers could be lost. Then, images C and D are masked with M obtaining images E and F, respectively; furthermore, a dissimilarity image is obtained by subtracting E and F. Finally, only differences in intensity greater than a threshold (e.g. 25, depending on the desired sensitivity) are pointed out. Their areas are also calculated: they are displayed in red in Fig. 7, in which areas are also reported (in blue), expressed in number of pixels or in 3D world coordinates.

Areas can be expressed in 3D world coordinates by means of the knowledge-based approach as done for the back-
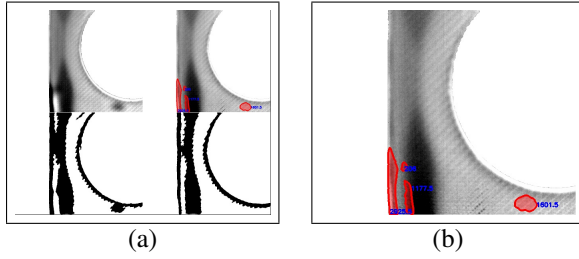
Fig. 7. (a) Comparison of a frame (upper right) with its reference (upper left) and their masks (bottom). (b) Zoom on defective areas, which are displayed in red and labeled in blue with their area expressed in number of pixels.
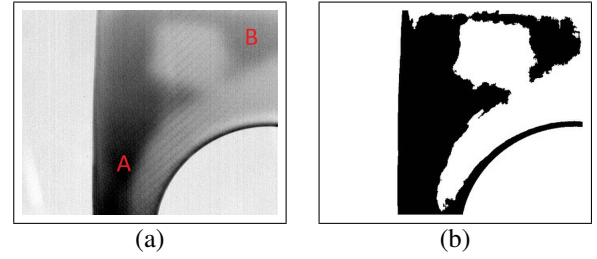

Fig. 8. (a) Example of frame with darks regions of different brightness, shape and size labeled by the letters A and B. (b) Corresponding mask: different kind of dark regions are detected.
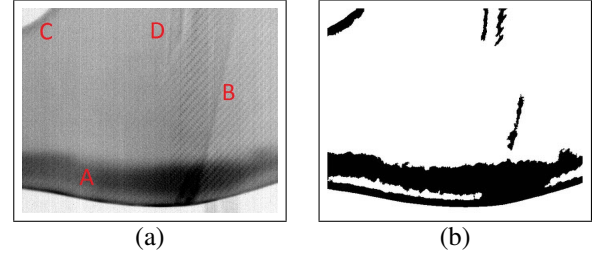

Fig. 9. (a) Example of frame with transients of different brightness, size and sharpness labeled by the letters A, B, C and D. (b) Corresponding mask: different kind of transitions are detected.

ground/foreground extraction. In this case, the four vertices of each pixel belonging to the foreground are projected to the 3D model and the area of the projected pixel is approximated by the area of a parallelogram in 3D world coordinates. Thus, the area of the defective region can be calculated as the sum of many parallelograms, each of which approximates the area covered by a pixel.

IV. EXPERIMENTAL RESULTS

This section deals with the application of the methods proposed in the previous section on a dataset provided by one of the project partners, Trimek S.A.. It contains 85 PPT phase images of 5 CFRP side blades from 17 points of view which cover the entire perimeter of the part. The frequency at which the PPT is evaluated depends on the acquisition duration and needs to be fine enough to enable discrimination of each signal of interest [13]. In our case, a good value was found to be 0.04 Hz. One of the 5 CFRP side blades is supposed not to have any defects and is taken as a reference for the comparisons so that each image can be analyzed and compared with the respective defect-free reference. In the following, the results are discussed: first of all, some remarks about the segmentation of the glue layer; second, the results of the 68 comparisons.

The detection of adhesive bondings in the extracted foreground must face with many types of dark regions with respect to the surrounding and light-dark transitions. There are some examples of dark regions of different brightness, shape and size labeled with the letters A and B in Fig. 8(a) and transients with different brightness, shape, size and sharpness labeled with the letters A, B, C and D in Fig. 9(a). As shown in Fig. 8(b) and 9(b), the proposed method can successfully detect several combinations: i) large or tapered dark regions, ii) dark regions and brightness transitions along the contours of the part, iii) sharp transitions due to local dishomogeneities in the glue layer. If contrast were adjusted globally, many details, which can be captured by the proposed local method, would instead be lost. Fig. 10 provides the comparison of the two methods: the first image (a) is the starting PPT phase image, the second (b) its global adjustment and the third (c) the mask obtained by USM.

To evaluate the performance of the whole system, the number of False Positives (FPs) and False Negatives (FNs) has been measured. Let A and B be the two images being compared, M the union of the two masks denoting the glue layers and D the detected defective areas: FPs may be caused by the noise or the carbon fibre pattern, both of which may differ in A and B. In addition, if the segmentation is not selective, M is large and areas without glue are compared potentially leading to FPs. Conversely, FNs occur if M does not completely cover the regions with glue. If those areas were different, they would not be revealed. In addition, given the experimental setup, the proposed method strongly relies on the assumption that the two parts are aligned. If this condition is not met in practice, there could be FPs or FNs. Two metrics are proposed here: $|M|$, which is the number of false positive or false negative pixels normalized by the number of pixels in M, and $|D|$, the same applied to D. The average values over the 68 comparisons and the worst/highest are reported in Table I. The best/lowest percentages are zero. Regarding false positives, the algorithm proves to work well with the exception of some ambiguous situations as that shown in Fig. 11, in which the reference frame (a), the second frame (b) and the output frame (c) are reported. In few comparisons, it can be hard to tell whether the ground truth or the algorithm is wrong. The region labeled with
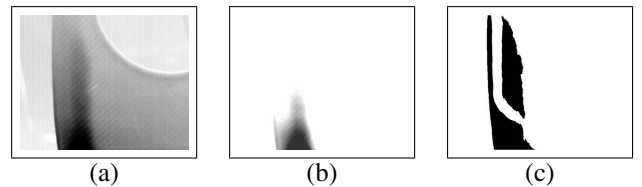

Fig. 10. Local differences, captured by local contrast adjustment, may be lost by adjusting contrast only globally: the first image (a) is the starting PPT phase image, the second (b) its global adjustment and the third (c) the mask obtained by unsharp masking.

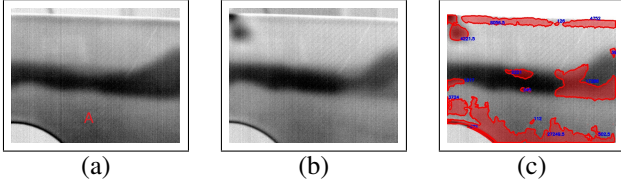| $FP/|M|$	$FP/|D|$	$FN/|M|$	$FN/|D|$
0.026	0.108	0.004	0.036
0.210	0.659	0.060	0.585

(a)   (b)   (c)

Fig. 11. Example of FPs: (a) reference PPT phase image: region A is dark (b) second frame (c) result of difference detection.

letter A in Fig. 11(a) is classified as defective but the ground truth does not consider that region as part of the glue layer even if it might be considered darker with respect to the surroundings. That region is quite large and causes high scores with both metrics. False negatives are instead very rare given that the segmentation phase works well and the algorithm robustly takes into account the union of the two masks. In Fig. 12, another comparison is reported.

The proposed method is very efficient in terms of computing time. The bottleneck is the post-processing, which finds small contours by border following and eliminate the respective small artifacts from the mask. On a common laptop with Intel Quad Core i5-3337U CPU @ 1.80 GHz, 8 GB of RAM and Windows 8.1, the average required time per image is 0.94 s, which is below the time required for the acquisition of the next PPT phase image, approximately 30 s.

V. CONCLUSIONS

This paper presented an autonomous robotic system for thermographic detection of defective areas in the superficial bonding layers of CFRPs taking a step forward compared to ongoing research. Indeed, previous work focused on the thermographic process, instead of the automatic thermo-image analysis. The proposed system uses a NDT&E technique named PPT, whose acquisition setup consists of a flash lamp and an infrared camera. The main point is the automatic thermo-image analysis, in particular the pairwise comparison of the acquired PPT phase images by means of automatic image processing techniques. It is performed in two steps: the segmentation of the adhesive bondings, which defines a region of interest, and the comparison of the pair of PPT phase images. The segmentation is based on local contrast adjustment via unsharp masking and is capable of dealing with ISO or vertical banding noise and artifacts due to the typical pattern of CFRPs, thanks to pre and post-processing
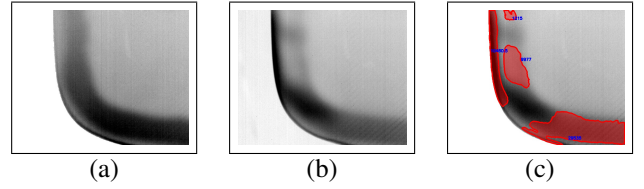

(a)   (b)   (c)

Fig. 12. Example of comparison: (a) reference PPT phase image (b) second frame (c) result of difference detection.

phases. Both steps take advantage from the high level of knowledge of the experimental setup. Many tests have been performed on PPT phase images taken from a number of points of view such that the entire perimeter of five CFRP side blades is covered. The proposed method has proven to be effective and efficient.

References

[1] DP Almond, B Weekes, T Li, SG Pickering, E Kostson, J Wilson, GY Tian, S Dixon, and S Burrows. Thermographic techniques for the detection of cracks in metallic components. *Insight-Non-Destructive Testing and Condition Monitoring*, 53(11):614–620, 2011.

[2] P Azad, T Gockel, and R Dillmann. *Computer Vision: principles and practice*. Elector International Media BV 2008, 2008.

[3] H Berglind and A Dillenz. Detecting glue deficiency in laminated wood - a thermography method comparison. *NDT & E International*, 36(6):395–399, 2003.

[4] L Boquete, S Ortega, JM Miguel-Jiménez, JM Rodríguez-Ascariz, and R Blanco. Automated detection of breast cancer in thermal infrared images, based on independent component analysis. *Journal of medical systems*, 36(1):103–111, 2012.

[5] G Bradski. The opencv library. *Doctor Dobbs Journal*, 25(11):120–126, 2000.

[6] S. Ghidoni, M. Antonello, L. Nanni, and E. Menegatti. A knowledge-based approach to crack detection in thermographic images. In *13th Int. Conf. on Intelligent Autonomous Systems (IAS-13)*, 2014. In press.

[7] S Goferman, L Zelnik-Manor, and A Tal. Context-aware saliency detection. *Pattern Analysis and Machine Intelligence, IEEE Transactions on*, 34(10):1915–1926, 2012.

[8] JF Head and RL Elliott. Infrared imaging: making progress in fulfilling its medical promise. *Engineering in Medicine and Biology Magazine, IEEE*, 21(6):80–85, 2002.

[9] C Ibarra-Castanedo, JM Piau, S Guilbert, NP Avdelidis, M Genest, A Bendada, and XPV Maldague. Comparative study of active thermography techniques for the nondestructive evaluation of honeycomb structures. *Research in Nondestructive Evaluation*, 20(1):1–31, 2009.

[10] M Ishikawa, H Hatta, Y Habuka, R Fukui, and S Utsunomiya. Detecting deeper defects using pulse phase thermography. *Infrared Physics & Technology*, 57:42–49, 2013.

[11] A Kelly. *Concise encyclopedia of composite materials*. Elsevier, 2012.

[12] X Maldague and S Marinetti. Pulse phase infrared thermography. *Journal of Applied Physics*, 79(5):2694–2698, 1996.

[13] S Marinetti, YA Plotnikov, WP Winfree, and A Braggiotti. Pulse phase thermography for defect detection and visualization. In *Nondestructive Evaluation Techniques for Aging Infrastructures & Manufacturing*, pages 230–238. International Society for Optics and Photonics, 1999.

[14] N Otsu. A threshold selection method from gray-level histograms. *Automatica*, 11(285-296):23–27, 1975.

[15] C Rother, V Kolmogorov, and A Blake. Grabcut: Interactive foreground extraction using iterated graph cuts. *ACM Transactions on Graphics (TOG)*, 23(3):309–314, 2004.

[16] RA Smith. Composite defects and their detection. *Materials Science and Engineering*, 3:103–143, 2009.

[17] S Suzuki. Topological structural analysis of digitized binary images by border following. *Computer Vision, Graphics, and Image Processing*, 30(1):32–46, 1985.

[18] W Swiderski and V Vavilov. Ir thermographic detection of defects in multi-layered composite materials used in military applications. In *Infrared and Millimeter Waves, 2007 and the 2007 15th International Conference on Terahertz Electronics. IRMMW-THz. Joint 32nd International Conference on*, pages 553–556. IEEE, 2007.